PAPER

First-principles prediction of the half-metallicity in quaternary Heusler CoRhCrAl thin films

Physica Scripta

PAPER

First-principles prediction of the half-metallicity in quaternary Heusler CoRhCrAl thin films

RECEIVED
25 February 2022

REVISED
28 May 2022

ACCEPTED FOR PUBLICATION
7 June 2022

PUBLISHED
16 June 2022

Iltaf Muhammad[1], **Yu He**[1], **Anwar Ali, Wen Zhang*** **and Ping Kwan Johnny Wong***

School of Microelectronics, Northwestern Polytechnical University, Xi'an 710072 & NPU Chongqing Technology Innovation Center, Chongqing 400000, People's Republic of China

[1] These authors contributed equally to this work.

* Authors to whom any correspondence should be addressed.

E-mail: pingkwanj.wong@nwpu.edu.cn **and** zhang.wen@nwpu.edu.cn

Keywords: Heusler alloys, electronic structures, magnetic properties, thin film, first-principles

Abstract

Magnetic thin films are essential building blocks for spintronic devices. Whether the spin-dependent properties associated with a parental bulk can be preserved at the surface or interface with a lowered symmetry represents an important topic to be addressed. In the work, theoretical calculations are performed to study the structural, electronic and magnetic properties of the bulk CoRhCrAl quaternary Heusler alloy and its (111)-, (001)- and (110)-oriented thin films by using the VASP package based on the first-principles density functional theory. Our results indicate that the bulk structure of CoRhCrAl alloy is half-metallic (HM) in character with 100% spin-polarization, and its spin-down bandgap and total magnetic moment are $E_g^{\downarrow} = 0.30$ eV and 3.00 μ_B, respectively. For the thin film structures with different orientations and terminations, half-metallicity only exists in the (111)-oriented thin film with Al-termination, but is lost in the Co-, Rh- or Cr-terminations. On the other hand, both the (001)- and (110)-oriented thin films are partially or nearly HM. Interestingly, the half-metallicity is lost on introducing U parameter in the calculations.

1. Introduction

Half-metals are ferro- or ferri-magnetic materials that act as conductors to electrons of one spin orientation, but as insulators or semiconductors to those of the opposite orientation. This exotic phenomenon, formally known as half-metallicity, gives rise to a 100% spin-polarization (SP) at the Fermi level E_F and was first identified in the Heusler alloy, NiMnSb, in 1983 [1]. Further exploration of other half-metals has received a strong boost, following the rise of spintronics, an exciting technology platform aiming at utilizing both spin and charge degrees of freedom to address the pressing demands for smaller, faster and more energy-efficient digital devices than conventional silicon-based electronics [2, 3]. In this context, the Heusler alloys have been considered as robust spin injectors or detectors in spintronic devices, as they possess the right mix of high Curie temperature in excess of room temperature and 100% SP [4]. This has indeed been demonstrated in some previous works realizing strong magnetoresistance effects in magnetic tunnel junctions with Co-based Heusler alloys [5].

The fragility of Heusler half-metallicity against atomic imperfections, such as structural disorder, represents a key challenge, however. It has been reported that more than 7% of atomic disorder is enough to vanish the half-metallic (HM) energy gap at the Fermi level E_F. Lowered symmetry at surface and interface represents another source of imperfection that could impact the HM bandgap. This is indeed the case for NiMnSb where a considerable discrepancy of the SP has been measured from the bulk single-crystals and thin films. As such, electronic band structure calculations remain as a leading tool for understanding the complicated physics of half-metallicity as well as the search for new half-metals. In addition, as thin films are mostly employed for device applications, it is logical to question whether the Heusler half-metallicity will be preserved at the surface or interface with lowered symmetry than the bulk counterpart. Salimi *et al* [6] reported that for the three kinds of (001)-oriented thin film structures with TiNi-, TiSn-, and NiSn-terminations respectively, only the TiSn-terminated (001)-oriented slab retains the excellent HM

Table 1. The three possible configurations of Y-type for the bulk CoRhCrAl quaternary Heusler alloy, the corresponding four Wyckoff positions are 4a (0, 0, 0), 4c (1/4, 1/4, 1/4), 4b (1/2, 1/2, 1/2) and 4d (3/4, 3/4, 3/4).

Y-type	Co	Rh	Cr	Al
Y1	4a	4c	4d	4b
Y2	4a	4b	4c	4d
Y3	4a	4c	4b	4d

properties of the bulk structure. As for quaternary Heusler alloy CoFeCrAl, only its artificial CrCr*-terminated (001)-oriented slab is expected to retain the half-metallicity while the CrAl- and AlAl-terminated (001)-oriented slabs are nearly HM [7]. Similar results are predicted for CoYCrZ (Z = Si, Ge, Ga, Al) [8, 9]. Meanwhile, the newly synthesized FeRhCrGe alloy and the theoretically studied FeRhCrSi alloy exhibit perfect HM at their equilibrium lattice constants with a total magnetic moment of 3.00 μ_B [10]. Recently, Patel *et al* [11–13] studied the electronic, magnetic and thermoelectric properties of various Heusler alloys.

In modern technology, as is well known, spin-based devices have gained particular interest owing to their advantages of low cost and fast processing speed over the conventional electronic devices. The prime importance of the present work is to explore the surface properties of the magnetic Heusler alloy, because in device fabrication, surface morphology and its chemistry together play a vital role in defining the performance of the device. In addition, surface effects often tend to destroy the bulk HM property, when a material is grown into thin film form. Here, in this paper, we use the Vienna *ab-initio* simulation package (VASP) based on DFT to study the structural, electronic and magnetic properties of bulk CoRhCrAl quaternary Heusler alloy as well as its thin films. Our results indicate the bulk alloy to be HM, with spin-down bandgap and total magnetic moment of 0.30 eV and 3.00 μ_B, respectively. The HM character is found to be carried by the (111)-oriented thin film with Al-termination, but is lost in the Co-, Rh- or Cr-terminations. On the other hand, the (001)- and (110)-oriented thin films both possess a partial or nearly HM character. We have also systematically examined the thermodynamical stability, Curie temperature, elastic constants, as well as other material parameters associated with the alloy to support our discussion.

2. Calculation method

To calculate the electronic and magnetic properties of bulk CoRhCrAl and its (111)-, (001)- and (110)-oriented thin films, we performed DFT calculations by VASP [14–17]. The projector augmented wave (PAW) method within the generalized gradient approximation (GGA) was carried out to represent the interaction between the ion core and the valence electrons [18, 19]. As for the electronic exchange-correlation, we adopted the Perdew–Burke–Ernzerhof (PBE) approach [20, 21]. The Brillouin zone of bulk CoRhCrAl and its (111)-, (001)- and (110)-oriented thin films were sampled by 7 × 7 × 7 and 7 × 7 × 1 K-point grids, respectively. A 0.05 eV Gaussian smearing broadening was used, along with a cut-off energy of 500 eV for the plane-wave basis set. The convergence tolerance for the iterative self-consistent loops was chosen to be 10^{-6} eV and the ions were fully relaxed until the maximum Hellmann–Feynman forces reaching 0.02 eV Å or smaller. The Co $3d^7 4s^2$, Rh $4d^8 5s^1$, Cr $3d^5 4s^1$, Al $3s^2 3p^1$ electrons were taken as valence electrons.

3. Results and discussions

3.1. Bulk structure

The quaternary Heusler alloy CoRhCrAl exhibits the LiMgPdSn-type crystal structure with space group $F\bar{4}3m$ (No. 216). The calculated equilibrium lattice constant of the bulk alloy is a = b = c = 5.87 Å, in good agreement with a previous study [22]. The four Wyckoff positions are 4a (0, 0, 0), 4c (1/4, 1/4, 1/4), 4b (1/2, 1/2, 1/2) and 4d (3/4, 3/4, 3/4), the Y-type has a total of three non-equivalent structures Y1, Y2, and Y3, each corresponding to a different lattice position, as shown in table 1 and figure 1(a). Besides, as the symmetry is provided by the space group, so any other way of atomic position exchange is structurally ineffective. The total energies of the ferromagnetic (FM) phase for the Y1, Y2 and Y3 structures of the CoRhCrAl quaternary Heusler alloys are −115.69 eV, −113.62 eV and −111.59 eV indicating that Y1 is the most stable configuration due to the lowest total energy. Furthermore, to optimize these three configurations, Jafari *et al* calculated the corresponding total energies as a function of lattice constants, and found the Y1 structure in the FM phase is the

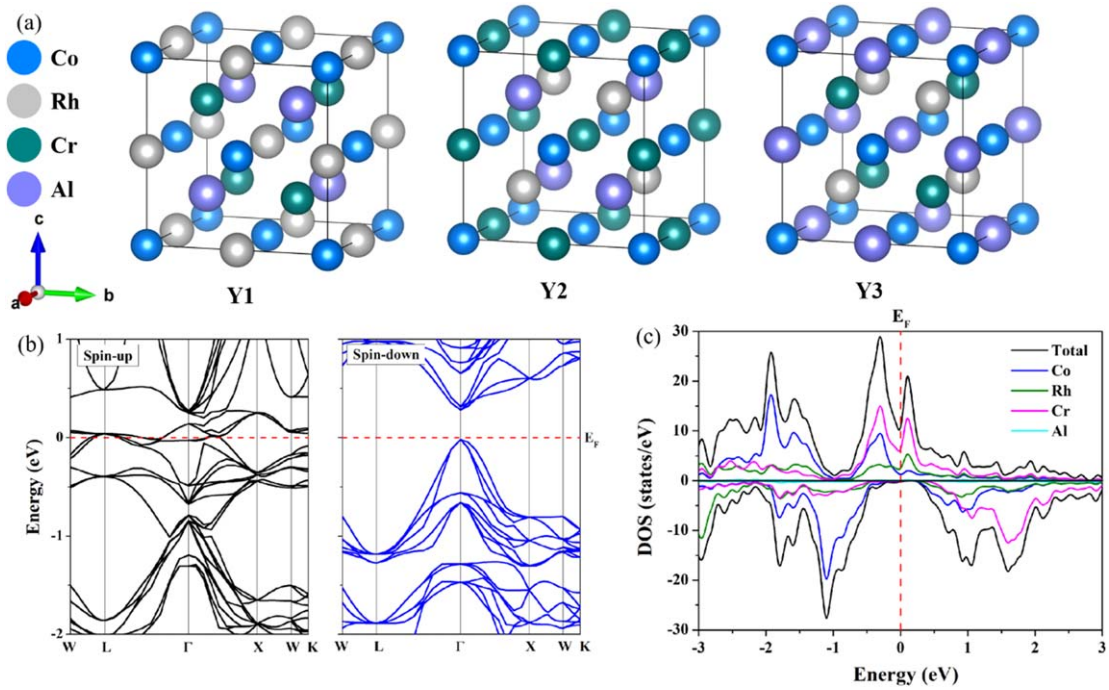

Figure 1. (a) The crystal structure of the bulk CoRhCrAl Heusler alloy with Y1, Y2, and Y3 configurations. (b) The spin-polarized band structure of the bulk CoRhCrAl Heusler alloy for Y1 configuration. The black and blue lines represent the spin-up and spin-down channels, respectively. The Fermi level E_F is set at zero energy and indicated by horizontal red dashed lines. (c) The total density of states (TDOS) (black lines) and partial density of states (PDOS) projected onto Co (blue lines), Rh (olive lines), Cr (magenta lines) and Al (cyan lines) atoms in the bulk CoRhCrAl Heusler alloy for Y1 configuration. The positive and negative values represent the spin-up and spin-down channels, respectively. The Fermi level E_F is set at zero energy and indicated by the vertical red dashed line.

Table 2. The lattice parameter a = b = c (Å), atomic magnetic moments μ_a (μ_B/atom), interstitial magnetic moments μ_{Int} (μ_B/f.u.), total magnetic moments μ_t (μ_B/f.u.), spin-down band gap $E_g^{\downarrow}$, the cohesive energies E_{coh} (eV), formation energies E_{form} (eV) and the Curie temperatures T_C (K) of the bulk CoRhCrAl quaternary Heusler alloy.

		μ_a									
Alloy	a	Co	Rh	Cr	Al	μ_{Int}	μ_t	$E_g^{\downarrow}$	E_{coh}	E_{form}	T_C
CoRhCrAl	5.87	0.96	0.08	2.02	−0.03	0.03	3.00	0.30	20.36	−0.38	618.33
[18]	5.88								−1.49	−0.10	

most stable [22, 23]. Therefore, the CoRhCrAl quaternary Heusler alloy in the FM phase with the Y1 configuration will be explored and analysed in the next sections.

Table 2 summarizes the cohesive and formation energies of the bulk CoRhCrAl. The cohesive energy (E_{coh}), which describes the force that holds atoms together in solids, can be computed as follows:

$$E_{coh} = (E_{Co}^{iso} + E_{Rh}^{iso} + E_{Cr}^{iso} + E_{Al}^{iso}) - E_{CoRhCrAl}^{total} \quad (1)$$

Where E_{Co}^{iso}, E_{Rh}^{iso}, E_{Cr}^{iso} and E_{Al}^{iso} represent the energies of isolated element atoms Co, Rh, Cr and Al, respectively while $E_{CoRhCrAl}^{total}$ is the equilibrium total energy of the bulk CoRhCrAl alloy. Formation energy E_{form} represents the energy required to disintegrate a material system into its individual components. Low formation energy means that the energy of the compound is stable, and can easily synthesize. The formation energy of the bulk CoRhCrAl alloy can be calculated by:

$$E_{form} = E_{CoRhCrAl}^{total} - (E_{Co}^{bulk} + E_{Rh}^{bulk} + E_{Cr}^{bulk} + E_{Al}^{bulk}) \quad (2)$$

Where $E_{CoRhCrAl}^{total}$ is the equilibrium total energy of the bulk CoRhCrAl alloy, and E_{Co}^{bulk}, E_{Rh}^{bulk}, E_{Cr}^{bulk} and E_{Al}^{bulk} represent the energies of the bulk Co, Rh, Cr and Al, respectively. According to table 2, the calculation results show that $E_{coh} = 20.36$eV and $E_{form} = -0.38$eV. The high cohesive energy indicates that the internal bond energy is high enough to obtain a stable compound, while the negative value of the formation energy indicates that the CoRhCrAl alloy is energetically stable and thus can be synthesized experimentally.

Table 3. The calculated elastic constants C_{ij} (GPa), bulk modulus B (GPa), shear modulus G (GPa), Young's modulus Y (GPa), Poisson's ratio ν, anisotropy A, Pugh's ratio B/G and Cauchy pressure C_p (GPa) of the bulk CoRhCrAl quaternary Heusler alloy.

Properties	
C_{11}	202.61
C_{12}	182.67
C_{44}	108.61
B	189.32
G	69.16
Y	184.95
ν	0.34
A	10.89
B/G	2.74
C_p	74.06

Table 4. The calculated density ρ (g/cm^3), longitudinal sound velocity v_l (m/s), transverse sound velocity v_s (m/s), average sound velocity v_m (m/s), Debye temperature Θ_D (K), minimum thermal conductivity κ_{min} (W/mK) and melting temperature T_{melt} (K) for the bulk CoRhCrAl quaternary Heusler alloy.

Alloy	ρ	v_l	V_s	v_m	Θ_D	κ_{min}	T_{melt}
CoRhCrAl	7866.71	5982.24	2964.98	3327.86	424.78	0.71	1730.45

The Curie temperature T_c is another key parameter that characterizes the stability of the FM phase against thermal energy, and can be calculated as follows:

$$T_c = \frac{\Delta E}{3K_B} \tag{3}$$

Where K_B represents the Boltzmann constant, $\Delta E = E_{AFM} - E_{FM}$ represents the energy difference of the CoRhCrAl alloy in the antiferromagnetic (AFM) and FM phases. As is shown in table 2, the calculated Curie temperature, $T_c = 618.33$K, is higher than room temperature, indicating that the quaternary Heusler alloy CoRhCrAl is suitable for applications of room temperature spintronics devices.

3.2. Mechanical stability and thermal properties

Both mechanical stability and thermal properties are analysed comprehensively here and are given in tables 3 and 4, respectively. By conducting six finite distortions of the lattice, the elastic stiffness constants C_{ij} of the bulk quaternary Heusler alloy CoRhCrAl can be derived from the strain stress relationship [24]. Meanwhile, it is important to note that, because of the high symmetry of the quaternary Heusler alloy, only the three independent elastic stiffness constants C_{11}, C_{12} and C_{44} are discussed in the following work. For cubic crystals, the calculated results are in well accordance with the mechanical stability criteria, which was proposed by M Born and K Huang [25]. Therefore, the bulk quaternary Heusler alloy CoRhCrAl is mechanically stable.

$$\begin{cases} C_{44} > 0 \\ \dfrac{C_{11} - C_{12}}{2} > 0 \\ B = \dfrac{C_{11} + 2C_{12}}{3} > 0 \\ C_{11} > B > C_{12} \end{cases} \tag{4}$$

The other derived calculation results as is shown in table 3, like the bulk modulus B (GPa), shear modulus G (GPa), Young's modulus Y (GPa), Poisson's ratio ν, anisotropy A, Pugh's ratio B/G and Cauchy pressure C_p (GPa) of the CoRhCrAl quaternary Heusler alloy, are estimated based on the Voigt-Reuss-Hill approximation

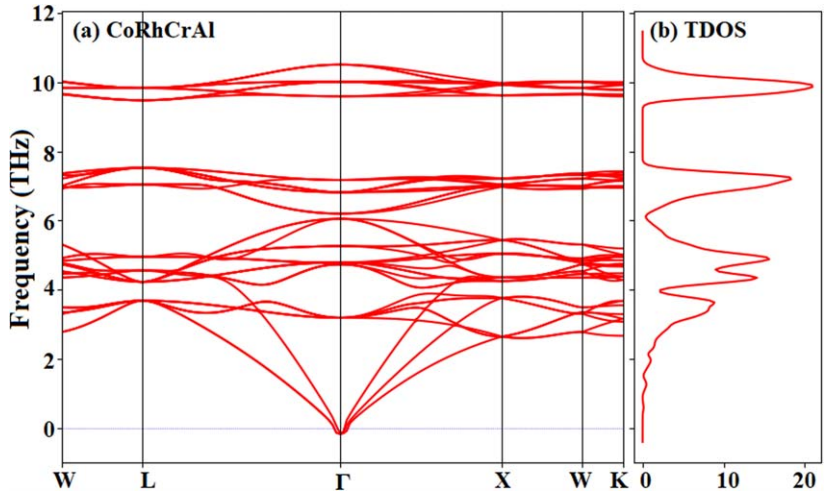

Figure 2. (a) Phonon dispersion curves and (b) the total phonon density of states TDOS of the CoRhCrAl quaternary Heusler alloy.

method [26] according to the formulas (5)–(10).

$$B = \frac{C_{11} + 2C_{12}}{3} \tag{5}$$

$$G = \frac{C_{11} - C_{12} + 3C_{44}}{5} \tag{6}$$

$$Y = \frac{9GB}{3B + G} \tag{7}$$

$$\nu = \frac{3B - 2G}{2(3B + G)} \tag{8}$$

$$A = \frac{2C_{44}}{C_{11} - C_{12}} \tag{9}$$

$$C_p = C_{12} - C_{44} \tag{10}$$

The Young's modulus Y is a physical parameter used to describe the resistance of solid materials to deformation under the influence of external forces, and can be calculated by these two intermediate variables, the bulk modulus B and the shear modulus G. The higher Young's modulus, the stiffer the material. Poisson's ratio ν, the ratio of transverse tensile strain to the tensile strain in the direction of tensile force, reveals the potential bonding relationship between atoms. The calculated Poisson's ratio ν of the CoRhCrAl quaternary Heusler alloys is 0.34, which is larger than 0.25, the typical Poisson's ratio for metal [27]. Therefore, it can be predicted theoretically that there are mainly metallic bonds within the CoRhCrAl compound alloy. Then the value of anisotropy A of CoRhCrAl is 10.89, indicating that this alloy is anisotropic. Apparently, the calculated Pugh's ratio B/G is 2.74, which is larger than 1.75 [28]. The Cauchy pressure $C_p = C_{12} - C_{44}$ is another key parameter for the bulk quaternary Heusler alloy. Both the large Pugh's ratio and positive Cauchy pressure indicate the nature of this alloy is ductile.

The three independent elastic stiffness constants C_{11}, C_{12} and C_{44} play an important role in the stiffness analysis, from which more parameters representing the thermodynamic properties of this alloy can be derived, according to table 4, the calculated density ρ, longitudinal sound velocity v_l, transverse sound velocity v_s, average sound velocity v_m, Debye temperature Θ_D, minimum thermal conductivity κ_{min} and melting temperature T_{melt}, etc. These parameters can be calculated as follows (formulas (11)–(16)):

$$v_l = \sqrt{\frac{3B + 4G}{3\rho}} \tag{11}$$

$$V_s = \sqrt{\frac{G}{\rho}} \tag{12}$$

$$v_m = \left[\frac{1}{3}\left[\frac{2}{V_s^3} + \frac{1}{v_l^3}\right]\right]^{-\frac{1}{3}} \tag{13}$$

$$\Theta_D = \frac{h}{k}\left[\frac{3n}{4\pi}\left(\frac{\rho N_A}{M}\right)\right]^{\frac{1}{3}} v_m \tag{14}$$

$$\kappa_{min} = k\left(\frac{nN_A\rho}{M}\right)^{\frac{2}{3}} v_m \tag{15}$$

$$T_{melt} = \left[553 + \left(\frac{5.91C_{11}}{GPa}\right)\right]k \pm 300k \tag{16}$$

where h is Planck constant, k is Boltzmann constant, N_A is Avogadro constant, M is the molecular weight of the solid and n is the number of atoms.

3.3. Dynamical stability

As for the dynamical stability of the bulk quaternary Heusler alloy CoRhCrAl, the phonon dispersion curves and the total phonon density of states TDOS are shown in figures 2(a) and (b), by using the PHONOPY package of VASP based on the first-principles DFT calculations [29], which is key to analyse the dynamical stability of the bulk quaternary Heusler alloy CoRhCrAl. Specifically, the linear response method of the density functional perturbation theory is used to obtain the corresponding vibrational frequencies and force parameter matrixes [30–32]. To calculate the force constants, a super-cell is constructed with the $7 \times 7 \times 7$ K-point grids and then the corresponding full phonon spectra are depicted along with the high symmetry directions in the irreducible Brillouin zone. As is shown in figure 2(a), the phonon dispersion curves can be categorized into two branches, the upper narrow optical branch (approximately at 10 THz) and the lower broad acoustic branch (approximately from 0 to 7.5 THz). Apparently, these phonon frequencies are all positive in character with the dynamical stability of this bulk alloy. There exists a gap between the two kinds of branches, in which the spin waves cannot propagate.

3.4. Bulk magnetic and electronic properties

The magnetic and electronic properties of bulk CoRhCrAl alloy are investigated here. As is shown in table 2, the total magnetic moments μ_t of the bulk CoRhCrAl alloy is 3.00 μ_B/f.u., following the Slater-Pauling rule $\mu_t = Z_t - 24$ [33–36], where Z_t is the total number of valence electrons. Around the Fermi level E_F, there is a spin splitting between the spin-up and spin-down channels of the TDOS resulting mainly from the d orbitals of the Co, Rh and Cr transition metal atoms, which results in magnetism of the alloy. According to the valence structures of Co $3d^74s^2$, Rh $4d^85s^1$, Cr $3d^54s^1$ and Al $3s^23p^1$, there are 27 valence electrons in CoRhCrAl alloy. From integrated values of the TDOS at Fermi level E_F, we find that there are 15 (12) spin-up (spin-down) electrons, respectively, *i.e.* $E_\uparrow = 15$ and $E_\downarrow = 12$. Therefore, the total magnetic moment of the CoRhCrAl alloy is $\mu_t = N_\uparrow - N_\downarrow = 15 - 12 = 3\ \mu_B$/f.u., satisfying the Slater-Pauling rule $\mu_t = Z_t - 24$ [22]. The atomic magnetic moments μ_a of the Co, Rh, Cr and Al are 0.96, 0.08, 2.02 and $-0.03\ \mu_B$/atom, respectively. The atomic magnetic moments μ_a show that the magnetic moment of the Cr atom contributes most to the total magnetic moment μ_t, while the magnetic moment of the Al atom is anti-parallel to those of Co, Rh and Cr atoms. Both the magnetic moments of the Rh and Al atoms are too small and are negligible. On the other hand, it should be noted that the sum of all atomic magnetic moments is less than the total magnetic moment μ_t, due to the existence of the interstitial magnetic moment μ_{Int}.

To analyse the electronic properties of the bulk CoRhCrAl alloy, the spin-polarized band structure is depicted in figure 1(b). The Fermi level E_F is set at zero energy and indicated by horizontal red dashed lines. In the spin-up channel, the energy band curves cross the Fermi level E_F, while in the spin-down channel $E_g^\downarrow$, there is a clear bandgap of 0.30 eV between the conduction band and valence band indicating that the bulk CoRhCrAl alloy is HM ferromagnet. The total density of states (TDOS) and partial density of states (PDOS) projected onto Co (blue lines), Rh (olive lines), Cr (magenta lines) and Al (cyan lines) atoms for the quaternary Heusler alloy CoRhCrAl are shown in figure 1(c). The positive and negative values represent the spin-up and spin-down channels, respectively. The Fermi level E_F is set at zero energy and indicated by a vertical red dashed line. The high TDOS below Fermi level E_F is mainly composed of d states of Co atoms, while in the spin-up channel, the TDOS around Fermi level E_F mainly comes from the d states of Cr and Co atoms. Obviously, the bandgap exists only in the spin-down channel while in the spin-up channel the TDOS shows metallic character, which also verifies the excellent half-metallicity in the bulk alloy. To study the role of hybridization in bulk CoRhCrAl alloy, the strong hybridization between d orbitals of transition metals (Co, Rh, and Cr) makes the d-orbitals split into bonding e_g. and t_{2g} orbitals (below the Fermi level E_F), non-bonding e_u and t_{1u} orbitals (around the Fermi level E_F), and anti-bonding e_g^* and t_{2g}^* orbitals (above the Fermi level E_F). This hybridization (known as d–d hybridization) is very effective in the formation of the spin-down band gap at the Fermi level E_F. The d–d hybridization is the origin of half-metallicity in the bulk CoRhCrAl alloy. On the other hand, the bonding states mainly belong to the high valent transition metals (Co and Rh) while the unoccupied antibonding states are

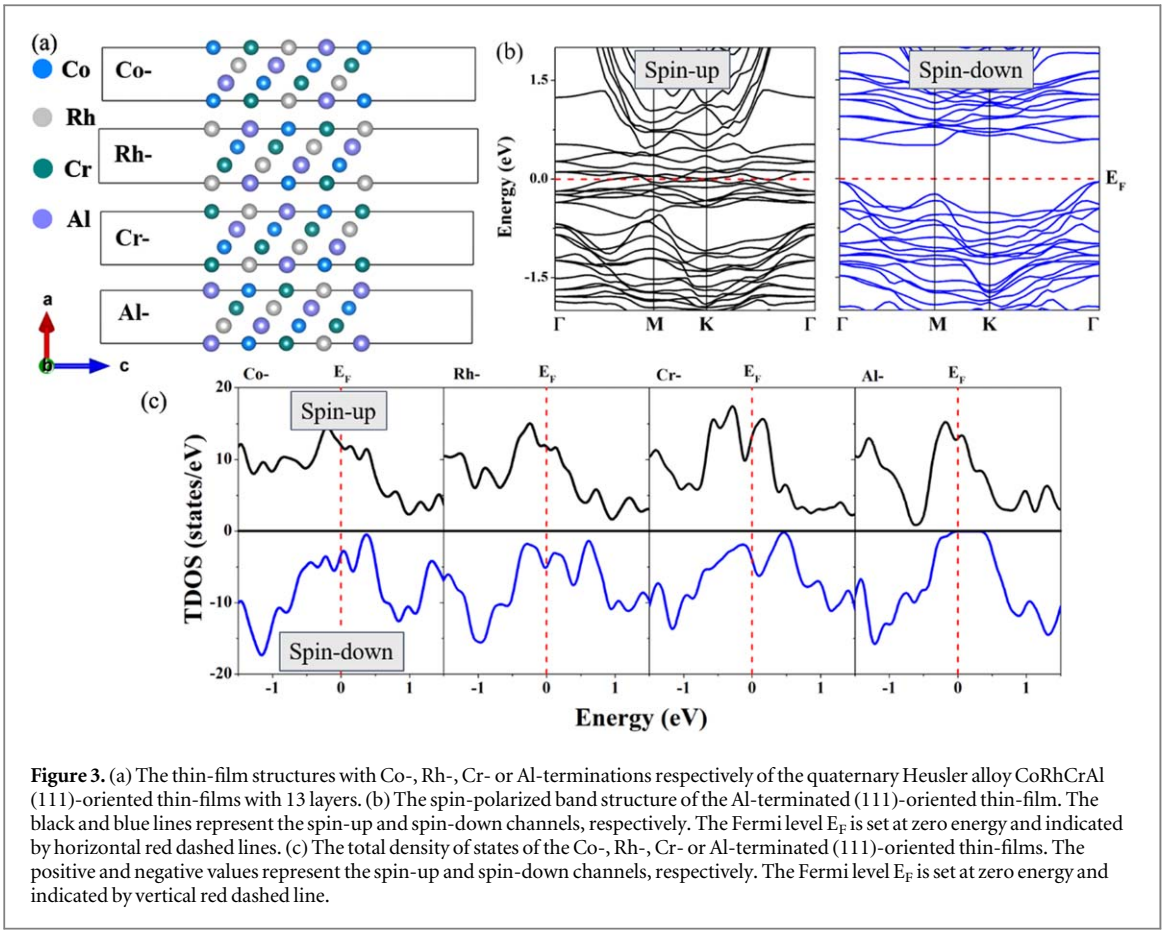

Figure 3. (a) The thin-film structures with Co-, Rh-, Cr- or Al-terminations respectively of the quaternary Heusler alloy CoRhCrAl (111)-oriented thin-films with 13 layers. (b) The spin-polarized band structure of the Al-terminated (111)-oriented thin-film. The black and blue lines represent the spin-up and spin-down channels, respectively. The Fermi level E_F is set at zero energy and indicated by horizontal red dashed lines. (c) The total density of states of the Co-, Rh-, Cr- or Al-terminated (111)-oriented thin-films. The positive and negative values represent the spin-up and spin-down channels, respectively. The Fermi level E_F is set at zero energy and indicated by vertical red dashed line.

Table 5. The spin-up $\rho^{\uparrow}$, spin-down $\rho^{\downarrow}$ states and spin-polarization SP (%) of the CoRhCrAl bulk and its (111)-, (001)-, and (110)-oriented thin-films with various terminations by GGA and GGA + U methods.

Slabs		GGA			GGA + U		
Orientations	Terminations	$\rho^{\uparrow}$	$\rho^{\downarrow}$	SP	$\rho^{\uparrow}$	$\rho^{\downarrow}$	SP
Bulk		13.34	0.00	100	15.51	1.59	81.40
(111)-	Co-	11.96	3.18	58.02	8.173	6.59	10.72
	Rh-	11.82	5.04	40.23	10.61	2.16	66.10
	Cr-	13.32	4.01	53.70	12.69	1.59	77.65
	Al-	12.96	0.00	100	8.34	4.46	30.23
(001)-	CoRh-	49.10	1.67	93.43	50.64	12.99	59.17
	CrAl-	45.46	1.99	91.63	60.34	22.39	45.87
(110)-	CoRhCrAl-	39.42	0.42	97.88	37.41	12.39	50.24

mainly relative to the low-valent transition metal atom Cr as shown in figure 1(c). This indicates hybridization between transition metals known as covalent hybridization which also leads to the appearance of a spin-down band gap. Furthermore, a weak hybridization between d states of transition metals with p states of Al, known as p–d hybridization, is also observed that can affect the width of the spin-down band gap [22]. In addition, according to the spin polarization (SP) formula:

$$\mathrm{SP} = \frac{\rho^{\uparrow} - \rho^{\downarrow}}{\rho^{\uparrow} + \rho^{\downarrow}} \tag{17}$$

Where $\rho^{\uparrow}$ and $\rho^{\downarrow}$ correspond to the spin-up and spin-down total density of states at Fermi level E_F. The bulk CoRhCrAl alloy exhibit 100% SP at the Fermi level E_F.

3.5. (111)-oriented thin film electronic properties

To simulate the (111)-oriented quaternary Heusler alloy CoRhCrAl thin film structures, we construct slabs containing 13 atomic layers with the vacuum of 15 Å to avoid interaction between successive slabs. Since each

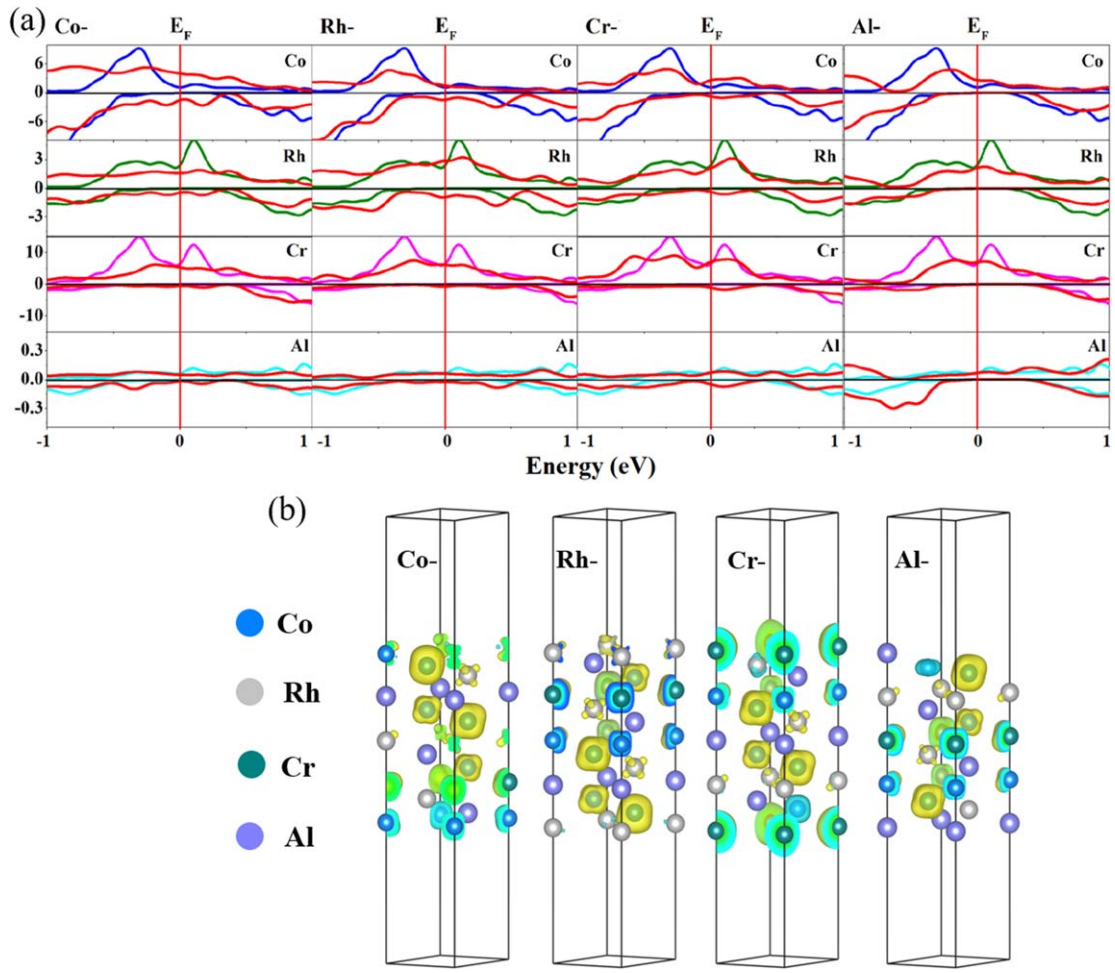

Figure 4. (a) The partial density of states (PDOS) projected onto the Co (red lines), Rh (red lines), Cr (red lines) and Al (red lines) atoms of the Co-, Rh-, Cr- or Al-terminations and the CoRhCrAl (111)-oriented thin-films along with Co (blue lines), Rh (olive lines), Cr (magenta lines) and Al (cyan lines) atoms of CoRhCrAl bulk. The red lines represent the PDOS of the surface while the other lines represent the bulk. (b) The magnetic charge densities of the Co-, Rh-, Cr- or Al-terminations respectively of the quaternary Heusler alloy CoRhCrAl (111)-oriented thin-films. The yellow isosurfaces represent a positive charge density (isosurfaces level) of 0.01 e/Å^3.

layer of the bulk CoRhCrAl along the [111] direction is composed of only one single element atoms respectively, the natural Co-, Rh-, Cr- and Al-terminations are thus formed by cleaving the bulk alloy CoRhCrAl along the selected direction, as shown in figure 3(a).

Firstly, the TDOS curves are depicted in figure 3(c) to analyse the electronic properties of the quaternary Heusler alloy CoRhCrAl (111)-oriented thin film structure with natural Co-, Rh-, Cr- or Al-terminations, respectively. Apparently, all the TDOS curves cross the Fermi level E_F in the spin-up channel, while in the spin-down channel, only the natural Al-terminated thin film structure possesses bandgap near the E_F. According to table 5, only the thin film structure with Al-termination exhibits 100% SP, retaining the excellent HM properties of the bulk structure. By employing vaspkit [37], the corresponding high-symmetry points are obtained for the spin-polarized band structure as is shown in figure 3(b). Similarly, in the spin-up channel, the energy band curves cross the Fermi level E_F, while in the spin-down channel, there is a clear bandgap between the conduction band and the valence band near the Fermi level E_F, indicating the nature of half-metallicity. Also, the results show that the spin-down bandgap and HM bandgap of the Al-terminated 111-oriented thin film structures are $E_g^{\downarrow} = 0.56$eV and $E_{HM} = -0.05$eV, respectively. The half-metallicity in the other three slabs with Co-, Rh- and Cr-terminations are destroyed due to surface states appearing in the vicinity of the Fermi level E_F. The HM property of the surfaces is sensitive to the surface chemical composition. Al atom is non-magnetic and thus can be regarded as less reactive than other constituent atoms, and thus tends to retain the HM property of the inner surface atoms. On the other hand, Co-, Rh- or Cr-terminated surfaces are more reactive and tend to share charge with neighboring atoms, resulting in the emergence of unstable energy states at the Fermi level E_F, which destroy the HM property. The PDOS projected onto the Co (red lines), Rh (red lines), Cr (red lines) and Al (red lines) atoms of the Co-, Rh-, Cr- or Al-terminations and the CoRhCrAl (111)-oriented thin films along with Co (blue lines), Rh (olive lines), Cr (magenta lines) and Al (cyan lines) atoms of CoRhCrAl bulk are depicted in figure 4(a).

Table 6. The spin-polarization SP (%) corresponding to the Co, Rh, Cr and Al atoms of the CoRhCrAl bulk and the (111)-, (001)-, and (110)-oriented thin-films with various terminations.

	Slabs				
Orientations	Terminations	Co	Rh	Cr	Al
Bulk		100	100	100	100
(111)-	Co-	45.01	55.56	84.15	47.97
	Rh-	0.80	49.56	80.26	45.50
	Cr-	54.88	70.11	74.98	21.97
	Al-	100	100	100	100
(001)-	CoRh-	77.30	96.96	98.02	94.16
	CrAl-	86.43	95.63	94.62	91.02
(110)-	CoRhCrAl-	96.64	98.17	99.02	94.24

The red lines represent the PDOS of the surface while the other lines represent the bulk. The SP of the corresponding Co, Rh, Cr and Al atoms in the CoRhCrAl bulk and the Co-, Rh-, Cr- or Al-terminated (111)-oriented CoRhCrAl slabs are listed in table 6. These results show that the SP of the Al-terminated (111)-oriented slab is similar to the bulk, thus preserving HM character while other slabs lost the HM character.

3.6. (111)-oriented thin film magnetic properties

To study the surface effect on the magnetic properties of the (111)-oriented thin film structure, the magnetic charge densities are depicted in figure 4(b), while the atomic magnetic moments at L_1, L_2 and L_c layers in the (111)-oriented thin film are listed in table 7. Obviously, for all thin films, the absolute values of the atomic magnetic moments M_a at layer L_c are almost the same as their bulk counterparts, showing that the slabs are thick enough to analyse the thin film properties. Similar to the bulk, the magnetic moments of Al and Rh atoms in each layer are negligible. From figure 4(b), the magnetic charge densities of the (111)-terminated thin film structures with Co-, Rh-, Cr- or Al-termination, respectively, the yellow isosurfaces represent positive charge density (isosurfaces level) of 0.01 e/Å^3. The isosurfaces surrounding the atoms represent the values of the magnetic charge density, corresponding to the magnetic moments of the atoms in the slabs. Cr atoms, for instance, possess the largest atomic magnetic moments M_a according to table 7, which indicates the main dominant contribution to the total magnetic moment. The negative charge densities are too small to be shown in this figure.

The origin of magnetization in the case of thin film is the occurrence of unsaturated dangling bonds at the surface, which opens the unpaired electrons which contribute to the magnetism. In the case of bulk materials, there is nothing like dangling bonds, rather the overlap of atomic orbitals results in spin splitting and thus a net magnetic moment. The interactions among neighboring atoms, result in charge transfer, which causes SP in the constituent atoms. In bulk materials, where each atom has a large coordination number than the surface atoms, the role of hybridization is strengthening the interaction between the atoms. The hybridized atomic orbitals (e.g. p orbitals with d-orbitals) overlap with each other, which can result in the decrease (increase) of SP in one (other) atom. For surfaces, the surface atoms do not have fully saturated bonds, and the hybridization is found to be weaker, which does not stabilize the surface states.

3.7. (001)- and (110)-oriented thin films electronic and magnetic properties

To simulate the (001)- and (110)-oriented thin film structures of the quaternary Heusler alloy CoRhCrAl, we use the Y1 configuration of the bulk in the FM phase to construct the slabs, with the (001)-oriented slabs containing 17 atomic layers while the (110)-oriented slabs containing 11 layers. All these slabs possess a vacuum of 20 Å to avoid interaction between successive slabs. The natural CoRh- or CrAl-terminations are formed by cleaving bulk CoRhCrAl along [001] direction, while the CoRhCrAl- termination is formed by cleaving along [110] direction, as shown in figure 5(a). The blue, silver-grey, olive green and medium slate blue balls represent Co, Rh, Cr and Al atoms, respectively. All atoms are allowed to relax during the structural optimization.

The TDOS of the CoRh- or CrAl-terminated (001)-oriented thin film structures, and the CoRhCrAl-terminated (110)-oriented thin film of the quaternary Heusler alloy CoRhCrAl are depicted in figure 5(b). The positive and negative values represent the spin-up and spin-down channels respectively and the Fermi level E_F is set at zero energy, denoted by vertical red dashed lines. The results show that the TDOS crosses the Fermi level E_F in both the spin-up and spin-down channel. It is worth noting that in the spin-down channel, there are small amount of states exists showing the nearly Hm character of these thin films. The SP of the CoRh- or CrAl-terminated (001)-oriented thin film structures are 93.43% and 91.63% respectively, while the SP of the

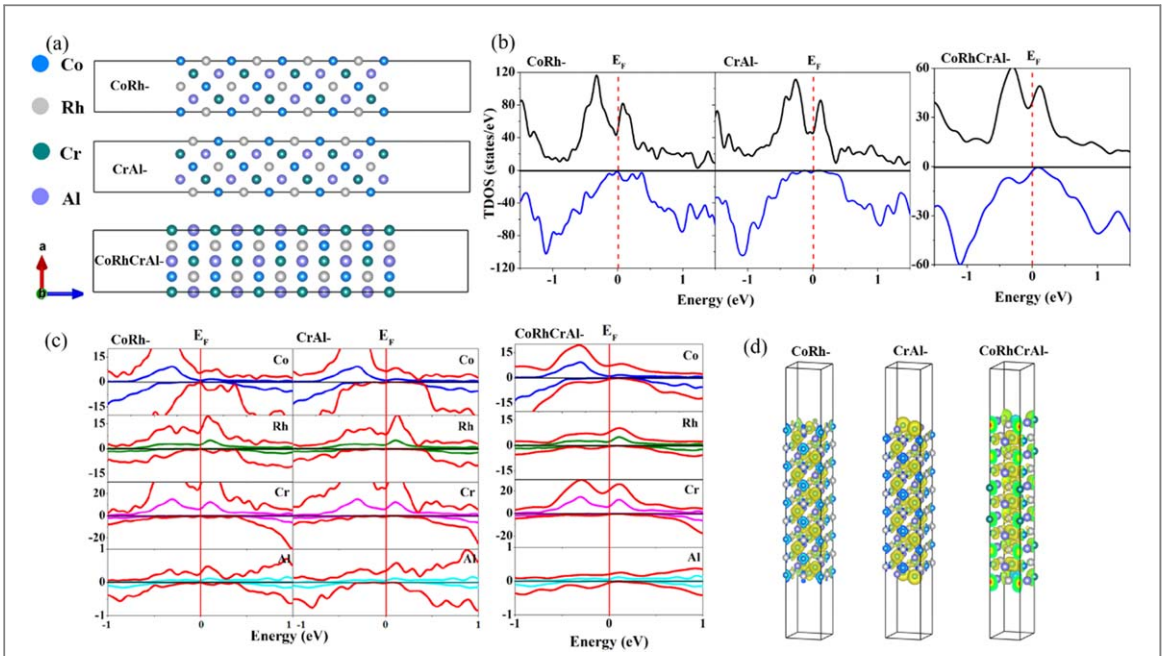

Figure 5. (a) The thin-film structures with CoRh- or CrAl-terminations of (001)-oriented thin films with 17 layers and CoRhCrAl-termination of (110)-oriented thin film with 11 layers. (b) the total density of states of the CoRh- or CrAl-terminated (001)-oriented thin-film structures, and the CoRhCrAl- terminated (110)-oriented thin film. (c) the PDOS projected onto the Co (red lines), Rh (red lines), Cr (red lines) and Al (red lines) atoms of the thin films along with Co (blue lines), Rh (olive lines), Cr (magenta lines) and Al (cyan lines) atoms of CoRhCrAl bulk. (d) The magnetic charge densities of the CoRh- or CrAl-terminated (001)-oriented thin-film structures, and the CoRhCrAl-terminated (110)-oriented thin film. The yellow isosurfaces represent a positive charge density (isosurfaces level) of 0.01 e/Å^3.

Table 7. The atomic magnetic moments (μ_B/atom) of L_1, L_2 and L_c layers in the (111)-, (001)-, and (110)-oriented thin-films.

		L_1		L_2		L_c	
Layers		Atoms	M_a	Atoms	M_a	Atoms	M_a
(111)-	Co-	Co	−0.86	Al	0.00	Rh	0.09
	Rh-	Rh	−0.00	Cr	2.38	Co	0.90
	Cr-	Cr	3.61	Co	−0.72	Al	−0.02
	Al-	Al	−0.04	Rh	−0.11	Cr	1.81
(001)-	CoRh-	Co	1.32	Cr	1.51	Co	0.95
		Rh	0.20	Al	−0.03	Rh	0.09
	CrAl-	Cr	3.61	Co	0.84	Cr	1.90
		Al	−0.01	Rh	0.21	Al	−0.03
(110)-	CoRhCrAl-	Co	−1.04	Co	0.84	Co	0.95
		Rh	−0.03	Rh	−0.01	Rh	0.09
		Cr	2.76	Cr	1.74	Cr	2.03
		Al	−0.03	Al	−0.03	Al	−0.03

CoRhCrAl-terminated (110)-oriented thin film is 94.24% as listed in table 5. Apparently, both the (001)- and (001)-oriented CoRhCrAl are nearly HM.

To further study the surface effect on the electronic properties of the (001)- and (110)-oriented thin film structure, the PDOS projected onto the Co (red lines), Rh (red lines), Cr (red lines) and Al (red lines) atoms of the thin films along with Co (blue lines), Rh (olive lines), Cr (magenta lines) and Al (cyan lines) atoms of CoRhCrAl bulk are depicted in figure 5(c). The vertical red lines are set at zero energy and represent the Fermi level E_F. The related atomic SPs corresponding to the Co, Rh, Cr and Al atoms of the (001)- and (110)-oriented thin film structures are listed in table 6. More intuitively, the magnetic charge densities of the CoRh- or CrAl-terminated (001)-oriented thin film structures, and the CoRhCrAl-terminated (110)-oriented thin film of the quaternary Heusler alloy CoRhCrAl are depicted in figure 5(d), in which the yellow isosurfaces represent positive charge density (isosurfaces level) of 0.01 e/Å^3. The related atomic magnetic moments of L_1, L_2 and L_c layers in the (001)- and (110)-oriented thin film structures are listed in table 7. All the results show that the (001)- and (001)-oriented CoRhCrAl are nearly HM.

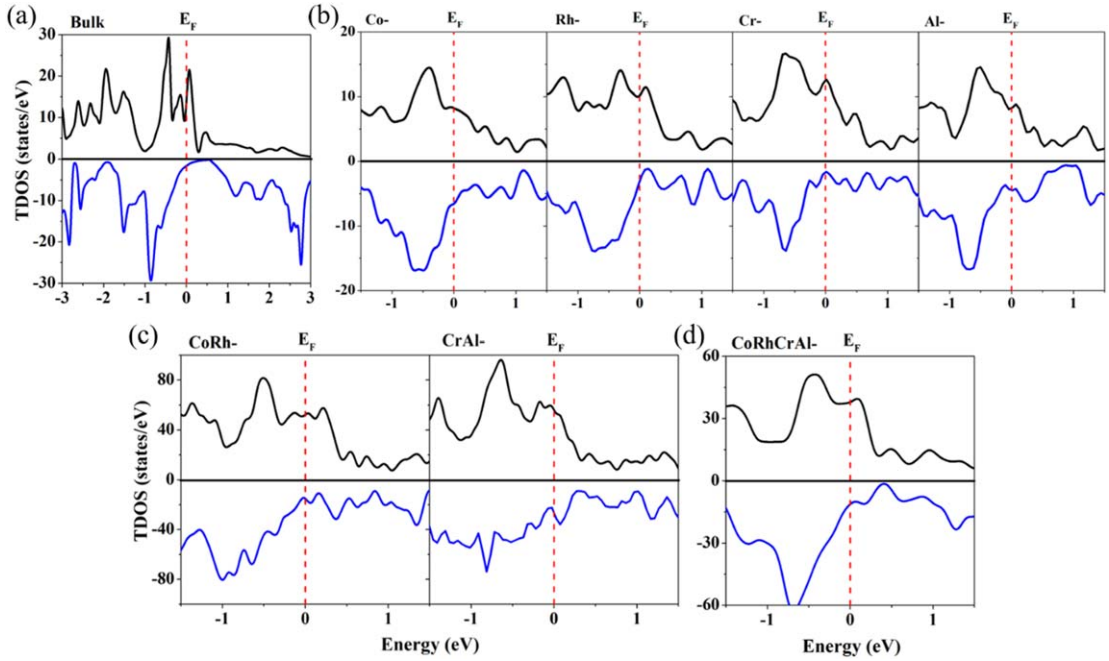

Figure 6. The total density of states (TDOS) of the (a) bulk CoRhCrAl quaternary Heusler alloy (b) Co-, Rh-, Cr- or Al-terminated (111)-oriented thin-films (c) the CoRh- or CrAl-terminated (001)-oriented thin-film structures and (d) the CoRhCrAl-terminated (110)-oriented thin film within GGA + U method.

To study the effect of Coulomb interaction U on the electronic properties of the bulk CoRhCrAl Heusler alloy and its (111)-, (001)- and (110)-oriented thin films, we calculate the TDOS within GGA + U [38] method (U = 2.0 eV for transition metals with d electrons) as shown in figures 6(a)–(d). Our results show that both the spin-up and spin-down states cross the Fermi level E_F, therefore, the HM character is lost for the bulk CoRhCrAl Heusler alloy and its (111)-, (001)- and (110)-oriented thin films within GGA + U method. The spin-up $\rho^{\uparrow}$, spin-down $\rho^{\downarrow}$ states and SP of the CoRhCrAl bulk and its (111)-, (001)-, and (110)-oriented thin films with various terminations by GGA and GGA + U methods are listed in table 5. Compared to GGA, the bulk CoRhCrAl Heusler alloy and its (111)-, (001)- and (110)-oriented thin films have more states in the vicinity of the Fermi level E_F in the spin-down channel, thus lost HM character within GGA + U calculations. The SP is found to be suppressed on introducing U parameter in the calculations. We expect the present work will stimulate further experimental efforts to investigate the electronic and magnetic properties of the bulk CoRhCrAl quaternary Heusler alloy and its thin films for spintronics and magnetoelectronics applications.

4. Conclusions

A first-principles study of the structural, electronic and magnetic properties of the bulk CoRhCrAl quaternary Heusler alloy and its (111)-, (001)- and (110)-oriented thin films are performed by using the VASP package based on DFT. The results indicate that the bulk CoRhCrAl alloy is HM in character with 100% SP. The SP of the Co-, Rh-, Cr- or Al-terminated (111)-oriented thin film structure are 58.02%, 40.23%, 53.70% and 100%, respectively, indicating that the HM character of the bulk CoRhCrAl alloy only exists in the (111)-oriented thin film with Al-termination, while it is lost in other terminations. Both the (001)- and (110)-oriented thin films are nearly HM, with the CoRh- or CrAl-terminated (001)-oriented thin films possessing 93.43% and 91.63% SP, respectively, whereas a SP up to 97.88% exists on the (110)-oriented thin film. Interestingly, the SP is found to be suppressed on introducing U parameter in the calculations.

Acknowledgments

The work is financially supported by the Natural Science Foundation of Chongqing (cstc2021jcyj-msxmX0740), Fundamental Research Funds for the Central Universities of China, the Natural Science Foundation of Shaanxi (2021JM-042, 2022JM-030) and NWPU Research Fund for Young Scholars (G2022WD01012, G2022WD01013), China.

Data availability statement

The data generated and/or analysed during the current study are not publicly available for legal/ethical reasons but are available from the corresponding author on reasonable request.

ORCID iDs

Iltaf Muhammad https://orcid.org/0000-0002-8304-2542
Ping Kwan Johnny Wong https://orcid.org/0000-0003-4645-0384

References

[1] de Groot R A, Mueller F M, Engen P G V and Buschow K H J 1983 New class of materials: half-metallic ferromagnets *Phys. Rev. Lett.* **50** 2024–7
[2] Elphick K, Frost W, Samiepour M, Kubota T, Takanashi K, Sukegawa H, Mitani S and Hirohata A 2021 Heusler alloys for spintronic devices: review on recent development and future perspectives *Sci. Technol. Adv. Mater.* **22** 235–71
[3] Liu W, Wong P K J and Xu Y 2019 Hybrid spintronic materials: Growth, structure and properties *Prog. Mater Sci.* **99** 27–105
[4] Hirohata A, Sagar J, Fleet L R and Parkin S S P 2016 *Heusler Alloy Films for Spintronic Devices BT - Heusler Alloys: Properties, Growth, Applications* ed C Felser and A Hirohata (Cham: Springer International Publishing) pp 219–48
[5] Sakuraba Y, Hattori M, Oogane M, Ando Y, Kato H, Sakuma A, Miyazaki T and Kubota H 2006 Giant tunneling magnetoresistance in Co2MnSi/Al-O/Co2MnSi magnetic tunnel junctions *Appl. Phys. Lett.* **88** 192508
[6] Salimi N, Boochani A, Elahi S M and Nevis Z G 2021 Investigation of electronic and thermoelectric properties of bulk and 001 thin film structures of half-heusler compound TiNiSn: a DFT study *Int. J. Thermophys.* **42** 77
[7] Muhammad I, Zhang J-M, Ali A and Muhammad S 2020 Preserving the half-metallicity at the quaternary Heusler CoFeCrAl (001)-oriented thin films: a first-principles study *Mater. Chem. Phys.* **240** 122262
[8] Khan M I, Arshad H, Rizwan M, Gillani S S A, Zafar M, Ahmed S and Shakil M 2020 Investigation of structural, electronic, magnetic and mechanical properties of a new series of equiatomic quaternary Heusler alloys CoYCrZ (Z = Si, Ge, Ga, Al): A DFT study *J. Alloys Compd.* **819** 152964
[9] Idrissi S, Labrim H, Ziti S and Bahmad L 2020 Investigation of the physical properties of the equiatomic quaternary Heusler alloy CoYCrZ (Z = Si and Ge): a DFT study *Appl. Phys. a-Materials Sci. Process.* **126** 190
[10] Khandy S A and Chai J D 2020 Thermoelectric properties, phonon, and mechanical stability of new half-metallic quaternary Heusler alloys: FeRhCrZ (Z = Si and Ge) *J. Appl. Phys.* **127** 165102
[11] Patel P D, Pillai S B, Shinde S M, Gupta S D and Jha P K 2018 Electronic, magnetic, thermoelectric and lattice dynamical properties of full heusler alloy Mn2RhSi: DFT study *Phys. B Condens. Matter* **550** 376–82
[12] Patel P D, Shinde S M, Gupta S D and Jha P K 2019 A promising thermoelectric response of fully compensated ferrimagnetic spin gapless semiconducting Heusler alloy Zr_2MnAl at high temperature: {DFT} study *Mater. Res. Express* **6** 76307
[13] Patel P D, Pandya J B, Shinde S M, Gupta S D, Narayan S and Jha P K 2020 Investigation of Full-Heusler compound Mn_2MgGe for magnetism, spintronics and thermoelectric applications: DFT study *Comput. Condens. Matter* **23** e00472
[14] Kresse G and Furthmüller J 1996 Efficiency of *ab-initio* total energy calculations for metals and semiconductors using a plane-wave basis set *Comput. Mater. Sci.* **6** 15–50
[15] Kresse G and Furthmüller J 1996 Efficient iterative schemes for *ab initio* total-energy calculations using a plane-wave basis set *Phys. Rev.* B **54** 11169–86
[16] Kresse G and Hafner J 1993 *Ab initio* molecular dynamics for open-shell transition metals *Phys. Rev.* B **48** 13115–8
[17] Kresse G and Hafner J 1994 *Ab initio* molecular-dynamics simulation of the liquid-metal-amorphous-semiconductor transition in germanium *Phys. Rev. B: Condens. Matter* **49** 14251–69
[18] Kresse G and Joubert D 1999 From ultrasoft pseudopotentials to the projector augmented-wave method *Phys. Rev.* B **59** 1758–75
[19] Vanderbilt D 1990 Soft self-consistent pseudopotentials in a generalized eigenvalue formalism *Phys. Rev.* B **41** 7892–5
[20] Hammer B, Hansen L B and Norskov J K 1999 Improved adsorption energetics within density-functional theory using revised Perdew–Burke–Ernzerhof functionals *Phys. Rev.* B **59** 7413–21
[21] Perdew J P, Burke K and Ernzerhof M 1996 Generalized gradient approximation made simple *Phys. Rev. Lett.* **77** 3865–8
[22] Jafari K and Ahmadian F 2017 First-principles study of magnetism and half-metallic properties for the quaternary Heusler alloys CoRhYZ (Y = Sc, Ti, Cr, and Mn; Z = Al, Si, and P) *J. Supercond. Nov. Magn.* **30** 2655–64
[23] Murnaghan F D 1944 The compressibility of media under extreme pressures *Proc. Natl. Acad. Sci. U. S. A.* **30** 244–7
[24] Le Page Y and Saxe P 2002 Symmetry-general least-squares extraction of elastic data for strained materials from *ab initio* calculations of stress *Phys. Rev.* B **65** 104104
[25] Matthew J A D 1970 Dynamical theory of crystal lattices by M Born and K Huang *Acta Crystallogr., Sect.* A **26** 702
[26] Hill R 1952 The elastic behaviour of a crystalline aggregate *Proc. Phys. Soc., Sect.* A **65** 349–54
[27] Haines J, Leger J M and Bocquillon G 2001 Synthesis and design of superhard materials *Annu. Rev. Mater. Res.* **31** 1–23
[28] Pugh S F 1954 XCII. Relations between the elastic moduli and the plastic properties of polycrystalline pure metals *London, Edinburgh, Dublin Philos. Mag. J. Sci.* **45** 823–43
[29] Muhammad I, Zhang J-M, Ali A, Rehman M U and Muhammad S 2019 First-principles prediction of the quaternary half-metallic ferromagnets TiZrIrZ (Z = Al, Ga or In) for spintronics applications *Thin Solid Films* **690** 137564
[30] Baroni S, de Gironcoli S, Dal Corso A and Giannozzi P 2001 Phonons and related crystal properties from density-functional perturbation theory *Rev. Mod. Phys.* **73** 515–62
[31] Giannozzi P, de Gironcoli S, Pavone P and Baroni S 1991 *Ab initio* calculation of phonon dispersions in semiconductors *Phys. Rev. B: Condens. Matter* **43** 7231–42
[32] Gonze X and Vigneron J P 1989 Density-functional approach to nonlinear-response coefficients of solids *Phys. Rev. B: Condens. Matter* **39** 13120–8
[33] Galanakis I, Dederichs P H and Papanikolaou N 2002 Slater-Pauling behavior and origin of the half-metallicity of the full-Heusler alloys *Phys. Rev.* B **66** 174429

[34] Galanakis I and Dederichs P H 2005 Half-metallicity and slater-pauling behavior in the ferromagnetic heusler alloys *Half-Metallic Alloys: Fundamentals and Applications* ed I Galanakis and P H Dederichs (Berlin, Heidelberg: Springer Berlin Heidelberg) pp 1–39
[35] Galanakis I, Mavropoulos P and Dederichs P H 2006 Electronic structure and Slater-Pauling behaviour in half-metallic Heusler alloys calculated from first principles *J. Phys. D-Applied Phys.* **39** 765–75
[36] Ozdogan K, Sasioglu E and Galanakis I 2013 Slater-Pauling behavior in LiMgPdSn-type multifunctional quaternary Heusler materials: Half-metallicity, spin-gapless and magnetic semiconductors *J. Appl. Phys.* **113** 193903
[37] Wang V, Xu N, Liu J-C, Tang G and Geng W-T 2021 VASPKIT: a user-friendly interface facilitating high-throughput computing and analysis using VASP code *Comput. Phys. Commun.* **267** 108033
[38] Anisimov V I and Gunnarsson O 1991 Density-functional calculation of effective Coulomb interactions in metals *Phys. Rev.* B **43** 7570–4